DOI: 10.1002/chem.200800547

Microsolvation Effects on the Optical Properties of Crystal Violet

Claire Loison,*[a] Rodolphe Antoine,[a] Michel Broyer,[a] Philippe Dugourd,[a] Julien Guthmuller,[a, b] and Daniel Simon[a]

Abstract: We present a joint experimental and theoretical study of the photoabsorption and photodissociation behavior of crystal violet, that is, the tris[*p*-(dimethylamino)phenyl]methyl cation. The photodissociation spectra of isolated and microsolvated crystal violet have been measured. A single band is observed for the bare cation. This is in good agreement with the calculated vibronic absorption spectrum based on time-dependent density functional theory calculations. The interaction of crystal violet with a single water molecule shifts and broadens the photodissociation spectrum, so that it approaches the spectrum obtained in solution. Theoretical calculations of the structure of the complex suggest that the shift in the absorption spectrum originates from a water molecule bonding with the central carbon atom of crystal violet.

Keywords: crystal violet · density functional calculations · octopolar molecules · photodissociation · solvent effects

Introduction

Crystal violet, the tris[*p*-(dimethylamino)phenyl]methyl cation, has been the subject of interest in various fields of science. For biologists, crystal violet is an important reactant to test whether bacteria are Gram-positive or -negative.[1–3] It is also a mutagen. For chemists, it is one of the most stable carbocations in aqueous solvents,[4] and is used as an organic dye for industrial applications.[5] For physicists, it can be used as a fluorescent tracer[6] or an octopolar molecule with a large first hyperpolarizability.[7–9] These remarkable optical properties have made this dye a prime candidate for nonlinear optical experiments,[10–12] near-field spectroscopy,[13] and single-molecule measurements.[14] The specificity of the electronic structure of crystal violet is due to its D_3 symmetry. Crystal violet has a propeller shape with three blades, and a zero electric dipole moment (see Figure 1).

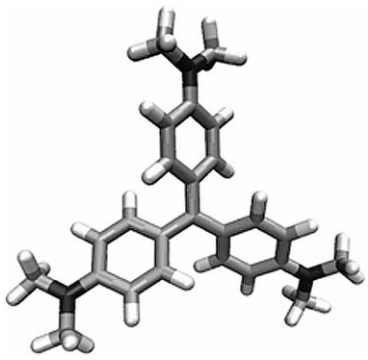

Figure 1. Geometry of CV^+ in a vacuum optimized by using DFT (B3LYP/6-31+G*) calculations. See the Experimental and Theoretical Section for details.

This symmetry of crystal violet has been confirmed in crystalline form by using X-ray diffraction;[15] and in solution by using Raman spectroscopy,[16] magnetic circular dichroism,[17] hyper-Rayleigh scattering,[18] and electronic structure calculations.[18–21] In the hydrate crystal $CV^+Cl^-\cdot 9H_2O$, in which CV^+ denotes crystal violet, the three dihedral angles between each aryl ring and the central carbon plane (θ_1, θ_2, and θ_3) are approximately 28°.[16] In the D_3 group, visible-light excitation should induce a single transition from a non-

[a] Dr. C. Loison, Dr. R. Antoine, Prof. M. Broyer, Prof. P. Dugourd, Dr. J. Guthmuller, Prof. D. Simon
Université de Lyon, Université Lyon 1; CNRS
LASIM UMR 5579
43 Bvd. du 11 novembre 1918, 69622 Villeurbanne (France)
Fax: (+33) 4-72431507
E-mail: claire.loison@lasim.univ-lyon1.fr

[b] Dr. J. Guthmuller
Present address: Laboratoire de Chimie Théorique Appliquée
Facultés Universitaire Notre-Dame de la Paix
Rue de Bruxelles 61, 5000 Namur (Belgium)

Supporting information for this article is available on the WWW under http://dx.doi.org/10.1002/chem.200800547.

degenerate S_0 ground state to a doubly degenerate S_1 state. However, experimental spectra of crystal violet in either crystalline form or solution reveal two closely spaced bands at $\lambda = 600$ nm. This feature is common to many substituted or unsubstituted triphenylmethyl cations.[19]

In the crystal, the presence of the counterions very close to crystal violet creates a high electric field that lifts the degeneracy of the S_1 excited state and could explain the doubling of the band.[16] In solution, ion pairing (in solvent with $\varepsilon < 10$) and aggregation (in solvent with $\varepsilon > 10$ and high dye concentration) also strongly influence the position and relative intensities of the two bands.[22,23] However, in the case of a dilute solution of crystal violet in water or methanol, counterion association or aggregation cannot be involved in symmetry breaking, yet the two bands remain. This has been a subject of debate since 1942, when Lewis and co-workers proposed the equilibrium between two rotational isomers in alcohol.[24] Today, this explanation has been invalidated[19] and other origins have been mentioned: 1) resolution of vibronic structures coming from a single electronic transition,[25] 2) symmetry breaking due to the interaction with the solvent,[19,23] 3) the existence of two isomers or two ground states in solution.[26] The first phenomenon would also be visible for isolated crystal violet, whereas the other two, which are due to a lowering of the symmetry resulting from intermolecular interactions, appear only if crystal violet is solvated or forms a complex with other molecules or ions. It is generally accepted that complexes between triphenylmethane dyes and a polar solvent like water or methanol possibly exist, however some controversy remains about the structure and optical properties of the complexes. McHale and co-workers argued that a dipolar solvent or counterions would lift the S_1 degeneracy without any change in the molecule geometry.[27] Maruyama and co-workers argued that the solvent would lift the D_3 symmetry of the ground state by pulling the central carbon atom out of the molecular plane.[26]

Herein, we report a joint experimental and theoretical investigation of the optical properties of isolated and microsolvated crystal violet cations. Isolated crystal violet displays one absorption band. A broader band with a shoulder, similar to that observed in solution, is measured for crystal violet microsolvated with a single water molecule.

Results and Discussion

Theoretical results for the UV-visible absorption of isolated crystal violet are first discussed and compared to the experimental photodissociation data. Then, the influence of the microsolvation with a single water molecule is discussed, using both theoretical and experimental investigations.

Crystal violet in the gas phase: The optimized geometry obtained for isolated crystal violet respects the D_3 symmetry group. The three dihedral angles between each aryl ring and the central carbon plane (θ) are close to 32° for all the functionals that were tested (B3LYP, BP, M05-2X). As expected from the chemical reactivity of the carbocation, the two degenerate HOMO orbitals of e symmetry (noted e_x and e_y) are delocalized on the aryl group with a substantial contribution on the nitrogen substituents, whereas the LUMO orbital of a_2 symmetry is delocalized on the aryl group with a substantial contribution on the central carbon (see Figure 2).

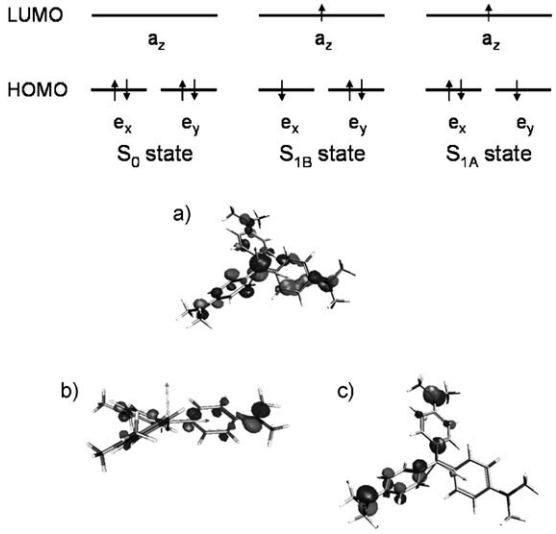

Figure 2. Top: electronic configurations for the S_0, S_{1A}, and S_{1B} states (S_{1A} and S_{1B} states are degenerate in D_3 symmetry and nondegenerate in C_{2v} symmetry). Bottom: a) LUMO, b) HOMO(x), and c) HOMO(y) of CV^+ calculated with B3LYP/6-31+G* in the D_3 symmetry group (dark and light gray shading show the different signs of the lobes).

Using the B3LYP-optimized geometry, TD-DFT-BP/ALDA (respectively SAOP/ALDA) calculations in the D_3 symmetry group predict two degenerate vertical excitations at 2.28 eV (respectively 2.33 eV) with an oscillator strength (f) of 0.56 (for both functionals). These excitations correspond to the $S_0 \rightarrow S_1$ electronic transition. The small energy difference obtained with the two functionals indicates that the long-range part of the SAOP functional almost cancels out in the present case, which is not obvious for such a conjugated cation with donor substituents. The two excitations are dominated by the two possible HOMO→LUMO transitions (the contribution of either $e_x \rightarrow a_2$ or $e_y \rightarrow a_2$ is more than 99%). The states obtained through the $e_x \rightarrow a_2$ and $e_y \rightarrow a_2$ transitions are denoted S_{1B} and S_{1A}, respectively (see Figure 2). Note that the following $S_0 \rightarrow S_2$ electronic transition energy is predicted to be at 3.90 eV, so this transition can certainly not explain the observed shoulder in the solution absorption spectrum.

A resolution of vibronic structures was suggested as an explanation for the shoulder in the spectra of crystal violet and also for the similar cation trioxatriangulenium (TOTA).[28] Since the excited-state electronic configuration $e^3a_2^1$ includes partially filled degenerate orbitals, some Jahn–Teller effect is expected. To test this idea, we optimized the

geometry of the excited singlet states (S_{1A} and S_{1B}) under the constraint of C_{2v} symmetry (with the principal axis along a bond between the central carbon atom and one of its three neighboring carbon atoms). As expected, deformations lower the energies of the S_{1A} and S_{1B} excited states. It was found that the two excited states relax toward two different geometries noted A and B. The respective deformations relative to the ground-state D_3 geometry, denoted ΔR_A and ΔR_B, involve 90 different vibrational modes, among which the antisymmetric change of the dihedral angles θ is a major component: for geometry B, $\Delta\theta_1=\Delta\theta_2=+6°$ and $\Delta\theta_3=-10°$; whereas for geometry A, $\Delta\theta_1=\Delta\theta_2=+1.5°$ and $\Delta\theta_3\approx-0.5°$. Figure 3 shows the energy variations of the S_0 and S_1 states as a function of the geometry of the molecule. The abscissa axes (q_A and q_B) are coordinates for linear transformations of the ground-state optimum geometry (noted D_3) toward the excited-states optimal geometries (either A or B). The Jahn–Teller effect slightly stabilizes the S_{1A} state along the q_A coordinate. The vertical transition energy toward this minimum is 2.23 eV. For the S_{1B} state, the stabilization along the q_B coordinate is more pronounced and the vertical transition energy toward this minimum is 2.10 eV.

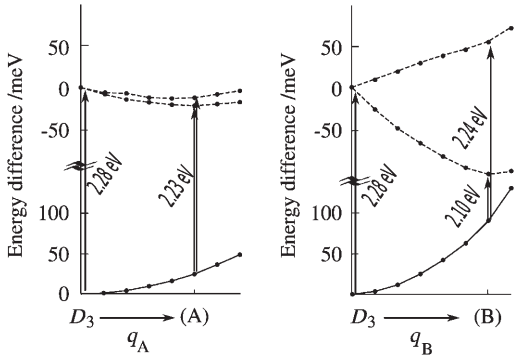

Figure 3. Plots of the total energy variations of the ground and two first excited singlet states as a function of the geometry of the molecule. The abscissa axes (q_A and q_B) are coordinates linearly transforming the ground-state optimum geometry (noted D_3) toward the excited-states optimal geometries (either A or B). For each geometry, the ground-state energies are given by (BP/ATZ2P) calculations and the excited-states energies are obtained with the addition of the TD-DFT (BP/ALDA/ATZ2P) transition energies to the ground-state energies. Note that there are two different zeros on the ordinate axes (for the ground state and for the excited states).

The calculated vibronic absorption spectrum of the $S_0\rightarrow S_1$ transition at 0 K is plotted in Figure 4, with contributions from the $S_0\rightarrow S_{1A}$ and $S_0\rightarrow S_{1B}$ transitions labeled as A and B, respectively. A single but asymmetric peak at $\lambda=555$ nm is observed. The effect of ambient temperature on the spectrum would a priori not change this conclusion. A peak at $\lambda=590$ nm or higher would only be expected if the $S_0\rightarrow S_{1B}$ vertical transitions around the B geometry were observable, which would require high temperatures (for the B geometry,

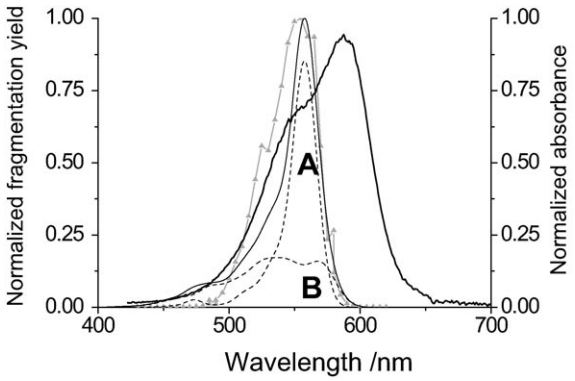

Figure 4. Experimental fragmentation yield of isolated CV^+ (▲) and normalized absorbance of CV^+ in solution (——) (4.7 μM CV^+ in H_2O/CH_3OH 60:40 (v/v) with 1% (v/v) of acetic acid). Calculated vibronic absorption spectrum (——) (each Franck–Condon factor was enlarged by a gaussian of width 0.05 eV). The contributions of the two HOMO→LUMO transitions (either HOMO(x)→LUMO or HOMO(y)→LUMO labeled B and A, respectively) are also plotted (-----).

the ground-state energy relative to the 0th vibration level is about 90 meV ≈ 1000 K, see Figure 3).

The experimental photodissociation spectrum for isolated crystal violet is shown in Figure 4. It displays a single absorption band centered around $\lambda=550$ nm. The calculated vibronic absorption spectrum for isolated crystal violet is in close agreement with the experimental photodissociation spectrum. As a comparison, the absorption spectrum of crystal violet in solution is also shown in Figure 4. This spectrum is much broader. It exhibits a shoulder pattern, composed of two bands. We used a two Gaussian band fit to extract the spectral characteristics of the absorption spectrum of crystal violet. The best-fit leads to a characteristic band centered on $\lambda=587$ nm and a weaker band at 539 nm (see the Supporting Information) with a full-width at half-maximum (FWHM) of 51.5 nm. The absorption band for isolated crystal violet is significantly narrower than that of the solution absorption spectrum (FWHM ≈ 50 nm). Furthermore, this band lies at the position of the smaller band of the solution spectrum, not at the position of the characteristic peak. Both the calculated vibronic absorption spectrum and photodissociation data definitely exclude the theory that the resolution of vibronic structures accounts for the observed shoulder in the solution absorption spectra of crystal violet.

As a conclusion, the experimental photodissociation spectrum of crystal violet without a shoulder is reported herein for the first time and is characteristic of an unsolvated environment. Our calculations show that the spectrum of unsolvated crystal violet should appear as a single, narrow S_0–S_1 peak; this has now been confirmed experimentally (see below).

CV^+–H_2O complex in the gas phase: Since the spectrum of isolated crystal violet shows a single peak, the shoulder pattern observed for crystal violet dissolved in water or methanol must be triggered by the interaction of crystal violet with its environment. The experimental photodissociation

cross section as a function of the excitation wavelength of the laser for the CV^+–H_2O complex is shown in Figure 5. The interaction of crystal violet with one single water mole-

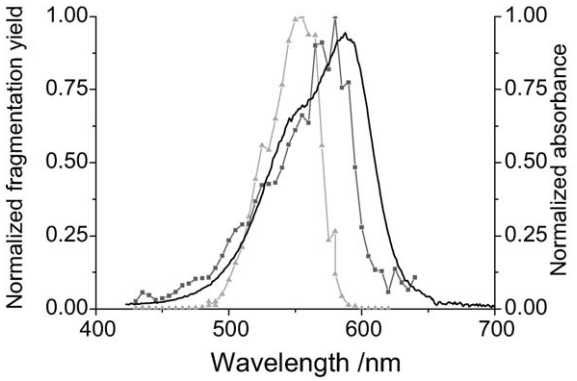

Figure 5. Plots of the experimental photodissociation cross sections as a function of the wavelength of the excitation laser for isolated CV^+ (▲) and CV^+–H_2O complex (■), superimposed with the normalized absorbance of CV^+ in solution (4.7 μM CV^+ in H_2O/CH_3OH 60:40 (v/v) with 1% (v/v) of acetic acid) (——).

cule shifts the maximum of the absorption band from 555 to 580 nm (i.e., from 2.24 to 2.14 eV). Therefore, the absorption peak of the CV^+–H_2O complex closely approaches the position of the maximum of the absorption band in solution (587 nm, that is, 2.11 eV). The interaction with water also broadens the main peak. Such broadening may arise from the presence of different isomers.

McHale and co-workers (INDO/S)[19] supported the idea that a polar molecule like methanol or water could break the symmetry without modifying the crystal violet geometry. They modeled the effect of solvent near another triphenylmethane cation, parafuchsine, by approaching it with a dipole moment or a charge. The position of this charge was arbitrarily chosen either above the central carbon atom or above one of the amino groups. A dipole of 1.4 D at a distance of 1.5 Å above the amino group would lift the degeneracy in qualitative agreement with the spectra of parafuchsine in methanol. Unfortunately, the dispersion interactions between the solvent and crystal violet, and the optical excitations were not precisely described by the methods used. New DFT functionals developed recently enabled us to propose enhanced insight into the geometries and optical signatures of CV^+–H_2O complexes. Starting from various initial states (including the states proposed by the groups of Maruyama and Lueck),[19,26] we optimized a representative sample of complex structures (see Figures 6 and 7). The total energies of the complexes relative to the isolated molecules and their transition energies are reported in Table 1.

In geometry **1**, the water molecule is located above the central carbocation (see Figures 6 and 7). This geometry does not correspond to a local energy minimum: despite a large sampling of initial geometries, water did not bind to the central carbon atom during the energy minimization procedures. Starting with water attacking the central carbon

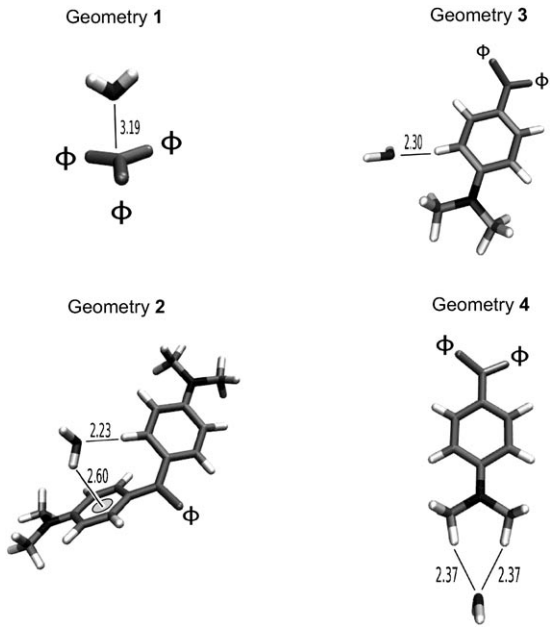

Figure 6. Geometries of four CV^+–H_2O complex structures. Hydrogen atoms are in white, nitrogen atoms in dark gray, and carbon atoms in gray. Only relevant parts of CV^+ are shown. Φ = aryl groups. Distances are given in Ångstrom.

atom with various distances and orientations, the complex always converged toward geometry **2**, in which the water molecule interacts with two different aryl rings. The total energy of the CV^+–H_2O complex was therefore calculated in a reduced space with two varying parameters (d, α), in which d is the distance between the oxygen atom of the water mole-

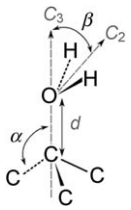

Figure 7. Some distances and angles defining the CV^+–H_2O complex in geometry **1**.

Table 1. Total energies (Q-chem3.1: M05-2X/6-31+G*) and transition energies (ADF2006: BP/ALDA/QZ4P) of the geometries of the CV^+–H_2O complexes illustrated in Figure 6. The energy reference (isolated CV^+ + isolated H_2O) is −1211.0671 Eh. The *xyz* files are available in the Supporting Information.

	Total energy differences [meV]	Transitions [eV] and oscillator strengths[a]
isolated CV^+ + isolated H_2O	0	2.321 (0.56)[b]
		2.326 (0.56)[b]
geometry **1**	−223	2.300 (0.54)
		2.343 (0.55)
geometry **2**	−272	2.318 (0.60)
		2.320 (0.54)
geometry **3**	−255	2.311 (0.57)
		2.321 (0.55)
geometry **4**	−280	2.318 (0.60)
		2.320 (0.54)

[a] In parentheses. [b] CV^+ geometry was optimized in C_1 symmetry group, so the two values are not exactly degenerate.

cule and the central carbon atom, and α is the angle between the C_3 axis and one of the C–C bonds (see Figure 7, in which β was fixed to 0). In this constrained space, an energy minimum was found for a distance between the oxygen atom of the water molecule and the central carbon atom of 3.19 Å, and a planar geometry around the central carbon atom ($\alpha = 90.5°$). A similar planar geometry was also obtained as a local energy minimum for the CV^+–MeOH complex (see the Supporting Information).

In geometry **2**, one hydrogen atom of water interacts with the aromatic electronic cloud of one aryl ring at a distance of 2.6 Å, which is typical for an aromatic π–H interaction.[29] The oxygen atom of water interacts with a lateral hydrogen atom of a neighboring ring at a distance close to 2.23 Å, which is within the range reported for $C_6H_6^+/H_2O$ complexes (2.1–2.6 Å).[30] Among the other local energy minima, water was found to bind to the hydrogen atoms of the aryl groups (geometry **3**), or to the dimethylamino substituents (geometry **4**). The attack of water towards the nitrogen atom, starting from several initial orientations, was unfavorable and converged toward geometry **2**. At ambient temperature ($k_BT \approx 30$ meV), one cannot exclude contributions from a mixture of different geometries, and deformation due to vibrations, in the ion trap. In solution, several of these binding sites could be occupied simultaneously.

For geometries **2** and **4**, the effect of water microsolvation on the transition energies is negligible. For geometry **3**, a small redshift is observed for one transition (10 meV). For geometry **1**, the splitting (43 meV) obtained at 0 K is smaller, but of the order of magnitude of the splitting observed experimentally. Obviously, other geometries may be responsible for the shoulder and for the broadening, which we could not find because of the limitations of geometry sampling. Nevertheless, it seems clear that a weak electrostatic interaction with the central carbocation contributes to the observed shift. Note that shifts in the S_0–S_1 band origin of the 1:1 water complexes of various phenols were observed and were correlated to changes in the charge on the phenolic oxygen atom.[31] In these complexes, the redshift is due to the electron-donating property of the water. For CV^+–H_2O complexes, water binding to the central carbon atom would be responsible for the observed shift.

To summarize, our theoretical investigation of CV^+–H_2O complexes indicates that water does not bind exclusively to the central carbon atom of crystal violet, but also to the external dimethylamino groups or to the aryl rings. Nevertheless, the binding to the central carbon atom seems to be mainly responsible for the broadening observed during microsolvation. Interactions with the central part of crystal violet may be at the origin of the shoulder in the absorption spectra of various substituted triphenylmethyl cations.

Conclusion

We have presented an experimental and theoretical work on the optical properties of crystal violet, both unsolvated and in interaction with a single water molecule. Experimentally, we first showed that unsolvated crystal violet presents a simple photodissociation spectrum with a single band, without the shoulder pattern observed in the absorption spectra of crystal violet in aqueous solution. This definitely demonstrates that the shoulder observed for crystal violet in solution is due to the environment. We made use of DFT and TD-DFT methods to study the ground state and the first doubly degenerate excited states. The calculated 0 K absorption spectra using the Franck–Condon approximation agrees well with the experimental photodissociation spectrum. A single peak is observed; that is, the Jahn–Teller effect of the excited states is not observable within the resolution used.

Additionally, we have been able to isolate CV^+–H_2O complexes in the gas phase. The experimental photodissociation spectrum of the CV^+–H_2O complex clearly shows that microsolvation redshifts and broadens the absorption spectrum of crystal violet, so that the position of the absorption peak closely approaches the position of the solution peak. By using theoretical calculations, we have investigated a range of possible complex geometries and their optical signature. The interaction of the solvent molecule with the central carbon atom of crystal violet may be responsible for the observed broadening of spectra in solution. In conclusion, this study shows that the intrinsic spectrum of crystal violet presents a single band and that the shoulder observed in solution is due to the environment. The main contributors to the effect of the interaction with the solvent are obtained at the very early stage of microsolvation.

Experimental and Theoretical Section

Electronic structure calculations

Ground state: electronic structure, geometry, and vibrational modes: The electronic structure calculations have been performed using DFT. The optimized geometry of crystal violet in a vacuum in the ground state has been obtained by the Gaussian 03 program[32] using the 6-31+G* basis set[33,34] and the B3LYP functional.[35,36] The vibrational frequencies and modes have been obtained analytically using Gaussian 03 with B3LYP/6-31G parameters.

For the computation of the energies of CV^+–H_2O complexes, which involve dispersion forces, the functional M05-2X,[37] as implemented in Qchem3.1, has been used with the 6-31+G* basis set. This hybrid meta-GGA functional has been designed for the study of noncovalent interactions and has proved successful in determining the geometries of complexes involving a water molecule and a conjugated organic molecule like benzene.[38] Geometries **2**, **3**, and **4** were optimized without constraint with Q-chem3.1 (M05-2X/6-31+G*) using default convergence parameters. Geometry **1** was chosen along an optimization path starting from a configuration in which water attacks the central carbon atom of crystal violet at a point close to a saddle point (gradient and energy change smaller than 10^{-5}).

Singlet excited states: The calculation of the excited singlet states has been determined with TD-DFT as implemented in the Amsterdam Density Functional program (ADF,[39] 2006). The exchange and correlation kernel is the adiabatic linear density approximation (ALDA).[40] We compare results obtained with the exchange by Becke and the correlation by Perdew (BP), and with the statistical average of orbital potential (SAOP) functional.[41] The latter has correct asymptotic behavior proportional to $-1/r$ when r tends to infinity (r is the distance between two charges), and

has shown to be well adapted for the calculation of excited energies of small organic molecules. Basis-set convergence was tested using Slater-type basis sets of increasing precision from the ADF library (DZ, DZP, TZ2P, ATZ2P, ET-pVQZ, and ZORA-4Q4P).[42,43] The largest basis set, ZORA-QZ4P, is a triple-zeta core and quadruple-zeta valence, with four polarization functions (2d and 2f functions for C and N; 2p and 2d for H) and can be considered as a very safe option for basis-set limit calculations. The transition energies obtained with basis set ATZ2P or larger converged within a range of 5 meV, and the oscillation strengths (*f*) converged within a range of 0.005. The HOMO–LUMO transition energies converged within 1 meV for a projection on at least the 20 lowest singlet excitations. This TD-DFT approach was first tested for a sample of nine octopolar cations similar to crystal violet (see the Supporting Information). The theoretical transition energies in a vacuum differed from the experimental ones (in solution) by less than 10%. This error is acceptable and in the range of what was published recently in a PCM-TD-DFT (PCM: polarizable continuum model) study of a large family of triphenylmethane derivatives including solvent effects.[44] A validation of the approach is also provided by the good agreement of the transition energies with the experimental photodissociation spectrum of isolated crystal violet presented in the Results and Discussion section of this paper.

Geometry optimization of the two singlet excited states (S_{1A} and S_{1B}): The geometries of the A and B excited states were optimized using a DFT approach (BP/ATZ2P) in which fractional occupation numbers of the orbitals are imposed and constrained during the optimization procedure. These occupation numbers describing the excited state are obtained from the decomposition of the $S_0 \rightarrow S_{1A}$ and $S_0 \rightarrow S_{1B}$ transitions of TD-DFT calculations. The two excited-state geometries noted A and B correspond to two deformations relative to the ground-state D_3 geometry noted ΔR_A and ΔR_B.

Vibronic resolution for isolated crystal violet: To take into account both electronic and vibrational states, the general expansion of the total wave function $\psi_{i,n}(r,R)$ is expressed within the adiabatic Born–Oppenheimer approximation [Eq. (1)]:

$$\psi_{i,n}(r,R) = \Phi_{i,n}(r,R) \times \chi_n^{(i)}(R) \quad (1)$$

in which $\Phi_{i,n}(r,R)$ is the *i*th electronic state wave function, and *r* and *R* denote electronic and nuclear coordinates, respectively. In the harmonic approximation used here, the nuclear wave function $\chi_n^{(i)}(R)$ is a product of wave functions of harmonic vibration modes denoted $n=(n_1, n_2, n_3, \ldots)$ with $\Sigma n_i = N$. We considered only the $0 \rightarrow n$ vibronic transition moment from the ground-state electronic state *i* to the final excited state $f\langle\psi_{i,0}(r,R)\,|\,\mu\,|\,\psi_{f,n}(r,R)\rangle$ within the Franck–Condon approximation. The vibronic transition moment can therefore be reduced to the product of the electronic dipole transition moment at the equilibrium geometry of the ground state with the vibrational overlap integral $\langle\chi_0^{(i)}(R)\,|\,\chi_n^{(f)}(R)\rangle$. As the absorption and fluorescence spectra of crystal violet respect a mirror symmetry, the harmonic vibrational modes of the excited states $\chi_n^{(f)}(R)$ were supposed to be the same as the one calculated for the ground state $\chi_n^{(i)}(R)$ centered on the excited-state geometries; for example, for the S_{1A} excited state $\chi_n^{(f)}(R) = \chi_n^{(i)}(R - \Delta R_A)$.[19,24] The calculation of Franck–Condon coefficients has been done with a program developed locally (MULTIFC).[45] For the A state, the geometry of which is close to the ground-state geometry, the calculation of about 3000 factors is sufficient to obtain a complete projection of the vibrational initial state.

$$\sum_n |\langle\chi_0^{(i)}(R)|\chi_n^{(f)}(R)\rangle|^2 > 0.99 \quad (2)$$

For the B state, whose geometry is very different from the ground-state geometry, the Franck–Condon factors are all tiny and the complete projection exceeds our computational resources. To reduce the computational cost, we projected the deformation ΔR_B on the 158 vibrational modes and eliminated 71 modes of negligible amplitude in the calculation. The number of Franck–Condon factors to be calculated was greatly reduced, while conserving an optimized projection on the vibrational modes. The projection of the 10^{10} biggest factors thus increased to

$$\sum_n |\langle\chi_0^{(i)}(R)|\chi_n^{(f)}(R)\rangle|^2 \cong 0.83 \quad (3)$$

The absorption spectra have been obtained in the frequency (ν) range, by summing the normalized contribution of all the Franck–Condon factors convoluted with a gaussian $\Delta\nu = 0.005$ eV wide defined by

$$\sum_n |\langle\chi_0^{(i)}(R)|\chi_n^{(f)}(R)\rangle|^2 \exp\left(\frac{-(\nu - E_n)^2}{\Delta\nu^2}\right) \quad (4)$$

in which E_n is the energy associated with the mode *n*.

Photodissociation experiments: Photodissociation experiments were performed using a modified commercial ion trap mass spectrometer (LCQ DUO with the MS^n option, Thermo Electron, San Jose, CA, USA) equipped with an on-axis electrospray source.[46–48] The ring electrode of the quadrupole ion trap was drilled to allow introduction of a laser beam. The laser used was a nanosecond frequency-doubled tunable Panther OPO laser pumped by a PowerLite 8000 Nd^{3+}:YAG laser (both from Continuum, Santa Clara, CA, USA) operated at a repetition rate of 20 Hz. Before entering the trap, the laser beam was collimated with three 3 mm diameter pinholes and went through a mechanical shutter that was electronically synchronized to the mass spectrometer.

Crystal violet was purchased from Sigma-Aldrich and dissolved at a concentration of 4.7 μM in H_2O/CH_3OH 60:40 (v/v); 1% (v/v) of acetic acid was added to the solution. Different settings for the LCQ mass spectrometer were used for the unsolvated crystal violet and for the CV^+–H_2O complex cations. For unsolvated crystal violet cations, the electrospray needle voltage was adjusted to −4 kV, and the spray was stabilized with a sheath gas pressure of 50 psi. The sample was introduced at 5 μL min^{-1}. The capillary interface was heated to a temperature of 250 °C. For crystal violet cations with one water molecule, the electrospray needle voltage was adjusted to −3 kV, and the spray was stabilized with a sheath gas pressure of 30 psi. The sample was introduced at 25 μL min^{-1}. The capillary interface was maintained at room temperature.

At each laser wavelength, the ions were first isolated in the trap and then irradiated with the laser for 2 s (40 laser pulses). The ions were finally ejected from the trap and the resulting mass spectrum was recorded in the *m*/*z* 100 to 400 range. For the isolated crystal violet and the CV^+–H_2O complex cations, the main observed photofragments correspond to the loss of CH_4 and of one of the three blades ($C_6H_5N(CH_3)_2$) (see the Supporting Information). Photofragmentation branching ratios do not depend on the laser wavelength and are similar to those obtained after collisional activation. Experiments performed as a function of the laser power show that photofragmentation is a one-photon process (see the Supporting Information). The photodissociation cross section was obtained by recording mass spectra at each wavelength from 430 to 640 nm by steps of 5 nm. The laser fluence injected in the trap was recorded before injection in the trap and kept below 1000 μJ pulse^{-1}. The cross section σ was determined by Equation (5):

$$\sigma = \frac{1}{\Phi}\ln\left(\frac{\text{parent} + \sum\text{products}}{\text{parent}}\right) \quad (5)$$

in which Φ is the laser fluence, "parent" is the intensity of the parent peak, and "Σproducts" is the sum of the intensity of all the observed photofragment peaks.

UV-visible spectra in solution were recorded by using an AvaSpec-2048 fiber optic spectrometer, an AvaLight-DH-S deuterium–halogen light source, and a UV/Vis cuvette (Avantes, Eerbeek Netherlands).

Acknowledgement

This work was supported by the Centre National de la Recherche Scientifique. The authors thank the Centre Informatique National de l'En-

seignement Supérieur (Montpellier) and the Pôle Scientifique de Modélisation Numérique (Lyon) for generous allocation of computer time.

[1] P. Plesiat, H. Nikaido, *Mol. Microbiol.* **1992**, *6*, 1323.
[2] D. A. Rouch, D. S. Cram, D. DiBerardino, T. G. Littlejohn, R. A. Skurray, *Mol. Microbiol.* **1990**, *4*, 2051.
[3] T. J. Beveridge, *Biotech. Histochem.* **2001**, *76*, 111.
[4] B. W. Laursen, F. C. Krebs, M. F. Nielsen, K. Bechgaard, J. B. Christensen, N. Harrit, *J. Am. Chem. Soc.* **1998**, *120*, 12255.
[5] L. Lewis, G. Indig, *Dyes. Pigm.* **2000**, *46*, 145.
[6] M. Ishikawa, J. Y. Ye, Y. Maruyama, H. Nakatsuka, *J. Phys. Chem. A* **1999**, *103*, 4319.
[7] T. Verbiest, K. Clays, C. Samyn, J. Wolff, D. Reinhoudt, A. Persoons, *J. Am. Chem. Soc.* **1994**, *116*, 9320.
[8] J. Zyss, *J. Chem. Phys.* **1993**, *98*, 6583.
[9] J. Zyss, T. Van, C. Dhenaut, I. Ledoux, *Chem. Phys.* **1993**, *177*, 281.
[10] G. Revillod, I. Russier-Antoine, E. Benichou, C. Jonin, P. F. Brevet, *J. Phys. Chem. B* **2005**, *109*, 5383.
[11] D. Beljonne, W. Weneleers, E. Zojer, Z. Shuai, H. Vogel, S. J. K. Pond, J. W. Perry, S. R. Marder, J.-L. Brédas, *Adv. Funct. Mater.* **2002**, *12*, 631.
[12] W.-H. Lee, H. Lee, J.-A. Kim, J.-H. Choi, M. Cho, S.-J. Jeon, B. R. Cho, *J. Am. Chem. Soc.* **2001**, *123*, 10658.
[13] N. Hayazawa, Y. Inouye, Z. Sekkat, S. Kawata, *J. Chem. Phys.* **2002**, *117*, 1296.
[14] K. Kneipp, Y. Wang, H. Kneipp, L. T. Perelman, I. Itzkan, *Phys. Rev. Lett.* **1997**, *78*, 1667.
[15] A. H. Gomes de Mesquita, H. C. H. MacGillavry, K. Eriks, *Acta Cryst.* **1965**, *18*, 437.
[16] S. Lovell, B. Marquardt, B. Kahr, *J. Chem. Soc. Perkin Trans. 2* **1999**, *2*, 2241.
[17] H. Dekkers, E. Kielmanvanluyt, *Mol. Phys.* **1976**, *31*, 1001.
[18] A. Kelley, L. Shoute, M. Blanchard-Desce, G. Bartholomew, G. Bazan, *Mol. Phys.* **2006**, *104*, 1239.
[19] H. Lueck, J. McHale, W. Edwards, *J. Am. Chem. Soc.* **1992**, *114*, 2342.
[20] C. Bourgogne, Ph.D. thesis, University Louis Pasteur, Strasbourg (France), **2000**.
[21] J. Fabian, H. Hartmann, A. Noack, *J. Phys. Org. Chem.* **2003**, *16*, 53.
[22] C. Oliveira, K. Branco, M. Baptista, G. Indig, *Spectrochim. Acta Part A* **2002**, *58*, 2971.
[23] J. Korppi-Tommola, E. Kolehmainen, E. Salo, R. W. Yip, *Chem. Phys. Lett.* **1984**, *104*, 373.
[24] G. N. Lewis, T. T. Magel, D. Lipkin, *J. Am. Chem. Soc.* **1942**, *64*, 1774.
[25] L. Angeloni, G. Smulevich, M. P. Marzocchi, *J. Mol. Struct.* **1980**, *61*, 331.
[26] Y. Maruyama, M. Ishikawa, H. Satozono, *J. Am. Chem. Soc.* **1996**, *118*, 6257.
[27] H. Lueck, D. Daniel, J. McHale, *J. Raman Spectrosc.* **1993**, *24*, 363.
[28] J. Reynisson, R. Wilbrandt, V. Brinck, B. W. Laursen, K. Norgaard, N. Harrit, A. M. Brouwer, *Photochem. Photobiol. Sci.* **2002**, *1*, 763.
[29] P. Tarakeshwar, H. S. Choi, S. J. Lee, J. Y. Lee, K. S. Kim, T. K. Ha, J. H. Jang, J. G. Lee, H. Lee, *J. Chem. Phys.* **1999**, *111*, 5838.
[30] Y. M. Ibrahim, M. M. N. Mautner, E. H. Alshraeh, M. S. El-Shall, S. Scheiner, *J. Am. Chem. Soc.* **2005**, *127*, 7053.
[31] M. Gerhards, B. Kimpfel, M. Pohl, M. Schmitt, K. Kleinermanns, *J. Mol. Struct.* **1992**, *270*, 301.
[32] Gaussian 03, Revision C.02, M. J. Frisch, G. W. Trucks, H. B. Schlegel, G. E. Scuseria, M. A. Robb, J. R. Cheeseman, J. A. Montgomery, Jr., T. Vreven, K. N. Kudin, J. C. Burant, J. M. Millam, S. S. Iyengar, J. Tomasi, V. Barone, B. Mennucci, M. Cossi, G. Scalmani, N. Rega, G. A. Petersson, H. Nakatsuji, M. Hada, M. Ehara, K. Toyota, R. Fukuda, J. Hasegawa, M. Ishida, T. Nakajima, Y. Honda, O. Kitao, H. Nakai, M. Klene, X. Li, J. E. Knox, H. P. Hratchian, J. B. Cross, V. Bakken, C. Adamo, J. Jaramillo, R. Gomperts, R. E. Stratmann, O. Yazyev, A. J. Austin, R. Cammi, C. Pomelli, J. W. Ochterski, P. Y. Ayala, K. Morokuma, G. A. Voth, P. Salvador, J. J. Dannenberg, V. G. Zakrzewski, S. Dapprich, A. D. Daniels, M. C. Strain, O. Farkas, D. K. Malick, A. D. Rabuck, K. Raghavachari, J. B. Foresman, J. V. Ortiz, Q. Cui, A. G. Baboul, S. Clifford, J. Cioslowski, B. B. Stefanov, G. Liu, A. Liashenko, P. Piskorz, I. Komaromi, R. L. Martin, D. J. Fox, T. Keith, M. A. Al-Laham, C. Y. Peng, A. Nanayakkara, M. Challacombe, P. M. W. Gill, B. Johnson, W. Chen, M. W. Wong, C. Gonzalez, J. A. Pople, Gaussian, Inc., Wallingford CT, **2004**.
[33] M. M. Francl, W. J. Petro, W. J. Hehre, J. S. Binkley, M. S. Gordon, D. J. DeFrees, J. A. Pople, *J. Chem. Phys.* **1982**, *77*, 3654.
[34] P. C. Hariharan, J. A. Pople, *Theor. Chim. Acta* **1973**, *28*, 213.
[35] A. D. Becke, *Phys. Rev. A* **1988**, *38*, 3098.
[36] C. Lee, W. Yang, R. G. Parr, *Phys. Rev. B* **1988**, *37*, 785.
[37] Y. Zhao, N. E. Schultz, D. G. Truhlar, *J. Chem. Theory Comput.* **2006**, *2*, 364.
[38] Y. Zhao, D. G. Truhlar, *J. Chem. Theory Comput.* **2007**, *3*, 289.
[39] T. Velde, F. M. Bickelhaupt, E. J. Baerends, F. Guerra, S. J. A. van Gisbergen, J. G. Snijders, T. Ziegler, *J. Comput. Chem.* **2001**, *22*, 931.
[40] A. Zangwill, P. Soven, *Phys. Rev. Lett.* **1980**, *45*, 204.
[41] P. R. T. Schipper, O. V. Gritsenko, S. J. A. van Gisbergen, E. J. Baerends, *J. Chem. Phys.* **2000**, *112*, 1344.
[42] D. P. Chong, E. van Lenthe, S. van Gisbergen, E. J. Baerends, *J. Comput. Chem.* **2004**, *25*, 1030.
[43] E. Van Lenthe, E. J. Baerends, *J. Comput. Chem.* **2003**, *24*, 1142.
[44] J. Preat, D. Jacquemin, V. Wathelet, J.-M. Andre, E. A. Perpete, *Chem. Phys.* **2007**, *335*, 177.
[45] J. Guthmuller, Ph.D. thesis, University Claude Bernard, Lyon (France), **2006**.
[46] F. O. Talbot, T. Tabarin, R. Antoine, M. Broyer, P. Dugourd, *J. Chem. Phys.* **2005**, *122*, 074310.
[47] T. Tabarin, R. Antoine, M. Broyer, P. Dugourd, *Rapid Commun. Mass Spectrom.* **2005**, *19*, 2883.
[48] L. Joly, R. Antoine, A. R. Allouche, M. Broyer, J. Lemoine, P. Dugourd, *J. Am. Chem. Soc.* **2007**, *129*, 8428.

Received: March 25, 2008
Published online: July 9, 2008

